

JOREK SIMULATION OF INJECTION ASSIMILATION AND RADIATION ASYMMETRY DURING ITER H-MODE DUAL SPIS

¹D.Hu, ²F.J. Artola, ³E. Nardon, ⁴M. Kong, ⁵D. Bonfiglio, ⁶M. Hoelzl, ⁶W. Tang, ^{3,7}G.T.A. Huijsmans, ¹Y. Yuan, ¹L. Cheng, ¹Y. Li & the ^aJOREK team

¹School of Physics, Beihang University, Beijing, China

²ITER Organization, Saint Paul-lez-Durance

³CEA, IRFM, Saint-Paul-lez-Durance, France

⁴École Polytechnique Fédérale de Lausanne (EPFL), Swiss Plasma Center (SPC), Lausanne, Switzerland

⁵Consorzio RFX and CNR-ISTP, Padova, Italy

⁶Max Planck Institute for Plasma Physics, Garching b. M., Germany

⁷Eindhoven University of Technology, De Rondom 70, 5612 AP Eindhoven, Netherlands

^aSee the author list of M. Hoelzl et al 2024 Nucl. Fusion 64 112016

Email: hudi2@buaa.edu.cn

One of the main purposes of the ITER Shattered Pellet Injection (SPI) system [1], is the mitigation of thermal loads during the Thermal Quench (TQ) phase of ITER disruptions. The SPI system achieves this by injecting Ne-doped H pellet fragments into the plasma. The impurities released from fragment ablation would then deplete the plasma thermal energy via line radiation, resulting in a more uniform energy deposition onto the plasma-facing-components (PFCs) as compared to the conduction and convection heat flux during unmitigated TQs. Nevertheless, the localized nature of SPI can also lead to localized radiating structures, which can result in detrimental line radiation loads on the PFCs. It is therefore crucial to assess the simultaneous thermal and line radiation loads mitigation at ITER, as well as to explore injection schemes that optimize material assimilation and favorable TQ conditions for runaway electron avoidance.

There have been extensive studies on the radiated fraction as well as the radiation asymmetry within the plasma volume after SPIS [2-5]. However, the ultimate criterion for the mitigation efficiency is the heat flux and accumulated energy impact on the first wall, as the latter is directly linked to the wall temperature rise [6]. As part of the ongoing efforts for the ITER PFC heat load predictions, JOREK collisional-radiative simulations of dual-SPIS into ITER baseline and so-called “degraded” H-mode, which mimics the H-L back transition during the disruption precursor phase [7], are carried out. The radiative heat flux onto the first wall is obtained through the Raysect/CHERAB code suite integrated within Integrated Modelling & Analysis Suite (IMAS) [8], and its energy impact over time is calculated by the convolution $\Delta Q(t) = \frac{1}{2} \int_{t_0}^t q_s(t')/\sqrt{t-t'} dt'$ [9]. Here t_0 is the beginning time of the heat pulse and $q_s(t)$ is the time dependent heat flux onto the first wall. The focus of this investigation is on exploring various dual-SPI configurations to find those that have high assimilation, low radiation asymmetry and energy impact below the PFC melting threshold.

Notation	Equilibria	Neon	Hydrogen	Frag.	Delay	Tor. Angle
BH-FP-dt0	baseline	$2 \times 2.5 \times 10^{22}$	$2 \times 1.8 \times 10^{24}$	300	0ms (asymm.)	180°
DH-FP-dt0	degraded	$2 \times 2.5 \times 10^{22}$	$2 \times 1.8 \times 10^{24}$	300	0ms	180°
DH-QP-dt0	degraded	$2 \times 2.5 \times 10^{22}$	$2 \times 4.5 \times 10^{23}$	100	0ms	180°
DH-QP-dt1	degraded	$2 \times 2.5 \times 10^{22}$	$2 \times 4.5 \times 10^{23}$	100	1ms	180°
DH-QP-dt0-ff	degraded	$2 \times 2.5 \times 10^{22}$	$2 \times 4.5 \times 10^{23}$	1000	0ms	180°
DH-QP-dt0-120	degraded	$2 \times 2.5 \times 10^{22}$	$2 \times 4.5 \times 10^{23}$	100	0ms	120°
DH-QP-stg	degraded	2×0 $+2 \times 2.5 \times 10^{22}$	$2 \times 5 \times 10^{23}$ $+2 \times 4.5 \times 10^{23}$	100 +100	0ms (staggered)	180°

Table 1, The injection parameters for the SPI considered in this study. BH and DH stand for the baseline and the degraded H-mode. Note that for BH-FP-dt0 there exists an asymmetry between the plumes although they are injected at the same time.

All the cases investigated in this study are summarized in Table 1, where the target equilibria, the neon and hydrogen injection quantities, the fragment numbers, the time delay between the dual-injectors and the toroidal angle between the dual-injectors are shown. For the staggered case, two plumes of fragments are injected from each injector. The first plume is pure hydrogen while the second is neon doped. The delay between the two plumes is 3.2ms, and the two injectors are perfectly synchronized for each plume. The total assimilation of neon and hydrogen, the radiated energy fraction, the TQ time defined from 90%-20% initial thermal energy, as well as the maximum energy impact onto the first wall for each case are summarized in Table 2. The relatively low assimilation and radiated fraction in the BH-FP-dt0 case are due to the strong plasmoid drift and accompanying MHD activity as the fragments arrive on the pedestal region [9].

Notation	Assim. Ne	Assim. H	f_{rad}	$t_{TQ}(90\%-20\%)$	Max. ΔQ
BH-FP-dt0	9.91×10^{21}	6.40×10^{23}	49.4%	2.0ms	$25.4MWs^{1/2}/m^2$
DH-FP-dt0	$\sim 1.1 \times 10^{22}$	$\sim 8.0 \times 10^{23}$	$\sim 76.5\%$	$\sim 3.1ms$	$16.0MWs^{1/2}/m^2$
DH-QP-dt0	2.53×10^{22}	4.40×10^{23}	89.8%	4.4ms	$5.7MWs^{1/2}/m^2$
DH-QP-dt1	2.15×10^{22}	3.58×10^{23}	86.3%	4.2ms	$14.9MWs^{1/2}/m^2$
DH-QP-dt0-ff	2.82×10^{22}	5.54×10^{23}	81.3%	2.4ms	$16.6MWs^{1/2}/m^2$
DH-QP-dt0-120	$\sim 2.5 \times 10^{22}$	$\sim 4.4 \times 10^{23}$	$\sim 84.5\%$	$\sim 4.4ms$	$11.6MWs^{1/2}/m^2$
DH-QP-stg	9.64×10^{21}	8.92×10^{23}	78.4%	7.91ms	$5.9MWs^{1/2}/m^2$

Table 2, The neon and hydrogen assimilation, radiated fraction, TQ time and maximum local energy impact for all cases considered in this section. The tilde signs indicate the estimated results extrapolated from the nearly-finished simulation results. Almost all of the non-radiative thermal energy loss in the DH-QP-stg case occurs during the H injection phase.

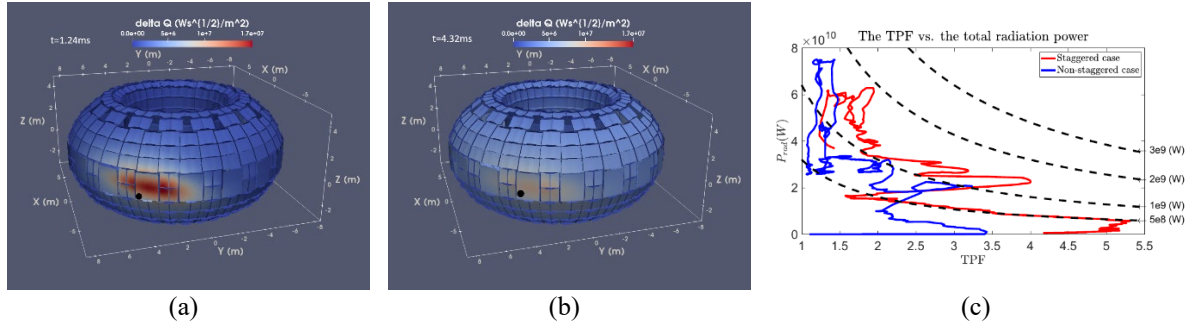


Figure 1, (a) The first wall energy impact of DH-QP-dt0-ff at $t = 1.24ms$ and (b) that at $t = 4.32ms$. The black dots mark the EQ-08 port. (c) The toroidal peaking factor for radiation power within the plasma volume versus the total radiation power for DH-QP-dt0 and DH-QP-stg. The black dashed lines represent different levels of maximum integrated radiation power within each poloidal planes used in the simulation, calculated by multiplying TPF to the toroidally averaged P_{rad} .

It is found that the radiation heat deposition tends to concentrate around the injecting ports in the early injection phase, while it spreads over larger areas towards the end of the TQ. An example of this is shown in Figure 1 (a) and (b) for the DH-QP-dt0-ff case. Another interesting observation is that stronger radiation asymmetry within the plasma would not necessarily translate into stronger energy impact on the first wall, as is shown in Figure 1 (c) where DH-QP-stg is shown to have higher radiation peaking factor compared with DH-QP-dt0, although their maximum energy impact are similar as is shown in Table 2.

Also shown in Table 2, in the baseline H-mode case, the energy impact stays well below the tungsten melting limit at $38MWs^{1/2}/m^2$ [6] although exceeding that of the stainless steel at $13MWs^{1/2}/m^2$ substantially [10]. Such melting is acceptable, as past experiments with similar level of energy impact indicate it would only result in slight surface roughening with no significant mass loss [10]. With the quarter pellet and degraded H-mode, the maximum radiation energy impact stays far below the tungsten limit [6] while approach that of the stainless-steel [10]. For the DH-QP-dt0 and DH-QP-stg case, milder MHD instabilities results in good synchronization which in turns further relaxes the energy impact distribution and reduce its maximum value, such that it never reaches the stainless-steel limit. These results are reassuring since they suggest the degraded H-mode cases could achieve high radiated fraction without the risk of melting the first wall. Further investigations including more realistic considerations such as the fragment rocket effect etc. are ongoing to further validate the ITER TQ disruption mitigation scheme.

REFERENCES

- [1] M. Lehnen, K. Aleynikova, P.B. Aleynikov et al., J. Nucl. Mater., **463**, 39-48 (2015);
- [2] S. Jachmich, U. Kruezi, M. Lehnen et al., Nucl. Fusion **62**, 026012 (2022);
- [3] B. Stein-Lubrano, R. Sweeney, D. Bonfiglio et al., Nucl. Fusion **64** 036020 (2024);
- [4] D. Hu, E. Nardon, F.J. Artola et al., Nucl. Fusion, **63**, 066008 (2023);
- [5] J. McClenaghan, B.C Lyons, C.C. Kim et al., Nucl. Fusion, **63**, 066029 (2023);
- [6] A. Herrmann, Plasma Phys. Control. Fusion **44** (2002) 883–903;
- [7] V. Riccardo, A. Loarte and the JET EFDA Contributors, Nucl. Fusion **45** 1427 (2005);
- [8] M. Carr et al., Raysect Python Raytracing Package (v0.4.0). Zenodo. <https://doi.org/10.5281/zenodo.1205064>;
- [9] D. Hu, F.J. Artola, E. Nardon et al., Nucl. Fusion **64** 086005 (2024);
- [10] N.S. Klimov, J. Linke, R.A. Pitts et al., J. Nucl. Mater., **438**, S241-S245 (2013);